Available online at www.sciencedirect.com
ScienceDirect
Journal of Power Sources 162 (2006) 388–399
JOURNAL OF POWER SOURCES
www.elsevier.com/locate/jpowsour

Model-based condition monitoring of PEM fuel cell using Hotelling T^2 control limit

X. Xue [a], J. Tang [a,*], N. Sammes [a], Y. Ding [b]

[a] *Department of Mechanical Engineering, University of Connecticut, 191 Auditorium Road, Unit 3139, Storrs, CT 06269-3139, United States*
[b] *Department of Industrial Engineering, Texas A&M University, College Station, TX 77843-3131, United States*

Received 30 May 2006; received in revised form 30 June 2006; accepted 3 July 2006
Available online 23 August 2006

Abstract

Although a variety of design and control strategies have been proposed to improve the performance of polymer electrolyte membrane (PEM) fuel cell systems, temporary faults in such systems still might occur during operations due to the complexity of the physical process and the functional limitations of some components. The development of an effective condition monitoring system that can detect these faults in a timely manner is complicated by the operating condition variation, the significant variability/uncertainty of the fuel cell system, and the measurement noise. In this research, we propose a model-based condition monitoring scheme that employs the Hotelling T^2 statistical analysis for fault detection of PEM fuel cells. Under a given operating condition, the instantaneous load current, the temperature and fuel/gas source pressures of the fuel cell are measured. These measurements are then fed into a lumped parameter dynamic fuel cell model for the establishment of the baseline under the same operating condition for comparison. The fuel cell operation is simulated under statistical sampling of parametric uncertainties with specified statistics (mean and variance) that account for the system variability/uncertainty and measurement noise. This yields a group of output voltages (under the same operating condition but with uncertainties) as the baseline. Fault detection is facilitated by comparing the real-time measurement of the fuel cell output voltage with the baseline voltages by employing the Hotelling T^2 statistical analysis. The baseline voltages are used to evaluate the output T^2 statistics under normal operating condition. Then, with a given confidence level the upper control limit can be specified. Fault condition will be declared if the T^2 statistics of real-time voltage measurement exceeds the upper control limit. This model-based robust condition monitoring scheme can deal with the operating condition variation, various uncertainties in a fuel cell system, and measurement noise. Our analysis indicates that this scheme has very high detection sensitivity and can detect the fault conditions at the early stage.

Keywords: PEM fuel cell; Condition monitoring; Dynamic model; Uncertainty; Measurement noise; Statistical analysis

1. Introduction

Polymer electrolyte membrane (PEM) fuel cell systems operate at relatively low temperatures and are promising candidates for future clean energy sources. These systems are intrinsically complex, with coupling effects of fluid, heat, electrochemical reaction, phase change, etc. There are also physical property limitations for fuel cell components such as membrane and electrodes. Therefore, fault conditions and even failure may occur under practical operating conditions. In fact, the reliability and durability are considered the main challenges to the fuel cell research community.

The fault conditions, which might be temporary or permanent, usually are closely related to a critical component of the fuel cell, the membrane-electrode assembly (MEA). Typically, three fault modes may be involved in fuel cell failures, i.e., the dehydration and drying of the membrane, the fuel/gas starvation of electrochemical reaction, and the leak of the membrane. It is well known that the electrolyte membrane needs to be appropriately hydrated in order to efficiently conduct the hydrogen protons and prevent the occurrence of localized hot spots. The dehydration and drying of the membrane lead to the increase of the internal resistance and a larger output voltage loss, which in turn raises the local temperature of the membrane. If the local overheating lasts for a long period of time, hot spot may occur and eventually permanently damage the membrane. Water transport across the membrane and water content therein depend on the combinational effects of the electro-osmotic drag force on

* Corresponding author. Tel.: +1 860 486 5911; fax: +1 860 486 5088.
E-mail address: jtang@engr.uconn.edu (J. Tang).

0378-7753/$ – see front matter © 2006 Elsevier B.V. All rights reserved.
doi:10.1016/j.jpowsour.2006.07.004

Nomenclature

a	water activity
A_{mem}	effective area of membrane (m^2)
c_i	specific heat $(J/(kg\,K)^{-1})$
C	water concentration ($mol\,m^{-3}$)
D_w	water diffusion coefficient ($m^2\,s^{-1}$)
F	Faraday's constant $(A\,s\,mol)^{-1}$
h_{latent}	latent heat of water phase change ($J\,kg^{-1}$)
hA	effective convection heat transfer coefficient
i	current density ($A\,m^{-2}$)
I	load current (A)
J_w	mole flux of water transport in the membrane $(mol(m^2\,s)^{-1})$
K_i	flow rate coefficient $(kg(Pa\,s)^{-1})$
m	species mass in the channels (kg)
M	species mole mass ($kg\,mol^{-1}$)
$M_{m,dry}$	mole mass of dry membrane ($kg\,mol^{-1}$)
n_d	electro-osmotic drag coefficient
N	number of cells in the stack
P	species partial pressure (Pa)
t_m	membrane thickness (m)
T	temperature (K)
V	channel volume (m^3)
W	flow rate ($kg\,s^{-1}$)

Greek symbols

β	humidity ratio
ϕ	relative humidity
λ	water content
$\rho_{m,dry}$	dry density of membrane ($kg\,m^{-3}$)
τ	time constant (s)
ξ_i	empirical coefficients of activation overvoltage

Superscripts and subscripts

an	anode
atm	ambient air
body	cell body
ca	cathode
cw	cooling water
hum	humidification
in	inlet
mem	membrane
O_2	oxygen
out	outlet
phase	phase change
s	source
sat	saturation
v	vapor
w	water

the water molecules and water back-diffusion from the cathode side to the anode side. It is believed that the electro-osmosis drag effect is larger than that of the back-diffusion, and the water content of the membrane is mainly dependent on that of the anode side [1–3]. If the fuel is not adequately humidified, the membrane may be dehydrated at the anode side, while flooding may occur at the cathode side due to water generated by the electrochemical reaction. The fuel/gas starvation might have several possible causes [1–4]. The first stage may be caused by the channel flow variation within the stack [4], i.e., the flow resistance directly resulting in the fuel/gas starvation in the channels, and consequently the electrolyte fuel/gas starvation. The reasons include the liquid water droplets forming in the flow channels, the temperature variation, and geometry deviation. The second stage fuel/gas starvation may be caused by the electrode pores blocked by the liquid water, which is termed "flooding". This phenomenon generally occurs at the cathode side. The fuel/gas starvation may interrupt the electrochemical reaction and lead to a rapid loss in the output voltage. In the worst situation, it may even lead to the decomposition of the fuel cell component and permanently damage the cells [3,4]. Another fault mode is the leak of the membrane, which is due to the fracture and/or hole of the membrane [4]. While the holes in the membrane may be caused by the hot spot, the fracture of the membrane is directly resulted from the mechanical stress concentration. Under the dynamic operating conditions, the pressure difference across the MEA may break the membrane [4].

In order to improve the reliability and the overall performance of PEM fuel cell systems, a number of design and control strategies have been proposed and some examples can be found in Refs. [5–8]. Currently, however, there exists very limited research on the monitoring and online fault detection of PEM fuel cells. Recently, Hissel et al. [9] explored a fuzzy diagnosis method for PEM fuel cells. A Sugeno-type fuzzy model of a PEM fuel cell was developed. The fuzzy model and the physical PEM fuel cell process, subjected to the same input, were placed in parallel to each other, and the output voltage difference between the model predication and the measurement was used to infer the fault occurrence. They considered the cases of accumulation of nitrogen and water in the anode compartment and the drying of the membrane. The main difficulty in the online monitoring for PEM fuel cells stems from the system complexity. While over the years PEM fuel cells have been modeled at various levels with different focuses, a global model capable of characterizing the dynamic and transient behavior of the fuel cells is still being pursued. Moreover, the modeling of certain components is based on phenomenological characterizations and the fuel cell system has inherent variability/uncertainty due to manufacturing tolerance, etc. These issues, together with the online measurement noise, make it very difficult to develop a *deterministic* model-based monitoring system. For example, a direct level-difference comparison between the online measurement and a deterministic baseline predicted by the dynamic model of a healthy fuel cell might lead to significant number of false alarms. Meanwhile, a fuel cell system normally operates under dynamic and varying conditions, e.g., constant changes in load current, temperature, flow rate, etc. Therefore, one would need to collect a huge amount of baseline data under all these varying conditions if a non-model based scheme is used, which would be extremely costly and even infeasible.

Building upon the previous studies and understandings mentioned above, in this paper we explore the development of a

model-based health monitoring strategy for PEM fuel cells using the statistical analysis. This proposed strategy can deal with the operating condition change and system uncertainty/noise simultaneously. Under a given operating condition, the instantaneous load current, the temperature and fuel/gas source pressures of the PEM fuel cell are measured. These measurements are then fed into a lumped parameter dynamic fuel cell model for the establishment of the baseline under the same operating condition for comparison. In order to account for the system variability/uncertainty, the fuel cell operation is simulated under statistical sampling of parametric uncertainties with specified statistics (mean and variance). This yields a group of output voltages (under the same operating condition but with uncertainties) as the baseline. Fault detection is facilitated by comparing the real-time measurement of the fuel cell output voltage with the baseline voltages from the statistical analysis standpoint. This proposed strategy involves two aspects of advancement. Building upon the recent progress, we first establish a system-level dynamic model of PEM fuel cell to characterize the complicated interactions of the temperature, gas flow, phase change in the anode and cathode channels, and membrane humidification under operating conditions. In this model, we explicitly take into account the phase change effect so that the water content and heat inside the PEM fuel cell, which are critical to the normal operation of the fuel cell, can be properly evaluated. At the fault detection stage, we incorporate the Hotelling T^2 statistics method [10] into the condition monitoring. The Hotelling T^2 statistics is a powerful tool of multi-variate statistical analysis, and has been widely used in process and quality controls [11,12]. Essentially, the T^2 value of the response data is used to measure the overall conformance to an established standard. In the proposed condition monitoring scheme for PEM fuel cell, the aforementioned baseline voltages obtained from the simulations under the same input are used to evaluate the output T^2 statistics under normal operating condition. Then, with a given confidence level the upper control limit can be specified. Fault condition will be declared if the T^2 statistics of real-time voltage measurement exceeds the upper control limit. A series of numerical studies are carried out to demonstrate the system performance. Our analysis shows that this proposed health monitoring system is capable of detecting fuel cell damage under complicated environment with system variability/uncertainty and measurement noise.

2. Health monitoring system development

2.1. Condition monitoring structure

The structure of the proposed health monitoring system is illustrated in Fig. 1. The main idea is to use the statistical analysis to compare the online measurement of the fuel cell output voltage to the baseline predicted by the healthy reference model. The reference model is placed in parallel to the physical fuel cell and is subjected to the same inputs. More specifically, the physical fuel cell variables such as fuel/gas source pressures, environment temperature, and load current will be measured using various sensors. All these measurement data will be used as inputs to the reference model. The healthy fuel cell output voltage prediction under the specific operating condition is then obtained using the fuel cell mathematical model. An important feature of the present research is that the system uncertainties/measurement noise will be taken into account. Generally, the system uncertainties stem from the modeling error as well as the cell-to-cell difference due to manufacturing tolerance. Mathematically, the system uncertainties can be characterized by perturbations (with certain mean and variance) to physical parameters involved in the fuel cell model. Therefore, in simulating the healthy fuel cell output voltage, we will run the reference model multiple times with statistical sampling of parametric uncertainties. A group of output voltages (with uncertainties/noise) can be obtained as the healthy fuel cell baseline. Fault detection is then facilitated by comparing the real-time measurement of the fuel cell output voltage with the baseline voltages by employing the Hotelling T^2 statistical analysis. The Hotelling analysis includes two stages, the baseline construction and the statistical analysis evaluation of the online measurement (monitored) data. At the phase one stage, the voltage outputs of the healthy fuel cell predicted by multiple simulations with system uncertainties/noise will be analyzed to establish/confirm the control limit under a given confidence level. A self-checking procedure is employed to either adjust the control limit (and the corresponding confi-

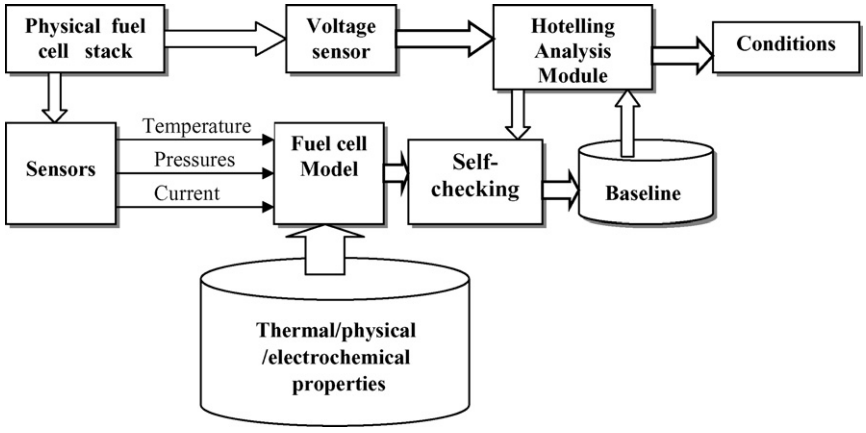

Fig. 1. Condition monitoring structure using Hotelling method.

dence level) for conformity or to eliminate the predictions with T^2 statistics exceeding the upper control limit. At phase two, when an online measurement of the output voltage is obtained for monitoring, it will be incorporated into the Hotelling T^2 analysis to establish a revised control limit that takes into account the increase of dimension of the dataset due to the inclusion of the new measurement. Statistically, the Hotelling T^2 analysis enables the conformity check between the voltage measurement and the baseline healthy voltage prediction. Fault condition will then be declared if the T^2 statistics of the online voltage measurement of the fuel cell being monitored exceeds the upper control limit. Clearly, this proposed condition monitoring system can deal with the two major issues in fuel cell applications, the complex multi-physics operation and the system uncertainties. The components shown in Fig. 1 will be explained in detail in what follows.

2.2. Reference model development

Without loss of generality, we use the Ballard Mark V 5 kW stack as benchmark example [13] and develop the mathematical model. The reason we choose this particular stack for demonstrating the methodology development is that the relevant parameters and typical operating processes are well-documented. The stack is composed of 35 cells. In a previous study, a general *system-level* modeling methodology for PEM fuel cell has been outlined [14]. In this section, we develop a mathematical model that is specifically tailored for stack health monitoring. It has been pointed out that, when only the stack voltage is used as information carrier, it is difficult to detect the failure of a single cell in a large stack [4]. The reason is that the wiring could become extremely complicated if one wants to measure single-cell output voltage. It is suggested that the group voltage monitoring of no more than five cells seems to be feasible from stack operation standpoint [4]. Therefore, in our study the stack modeling will be based on the group consideration of five cells. The dry fuel from a compressed gas tank and the dry purified air from an air compressor enter the stack separately and flow directly into the humidification section where the fuel/gas streams pick up water. The fuel/gas main streams are further separated and then individually fed into each of the fuel cells in their respective anode and cathode channels in the active fuel cell section. The electrochemical reaction takes place at the individual MEA. The electrical power is then generated, and the surplus fuel/gas and produced water due to the electrochemical reaction flow out through their respective outlets.

PEM fuel cell has been modeled at various levels of complexity [1–3,14–17]. While the micro-level models of single cell aim at the cell component synthesis/design, these models consist of complex partial differential equations and are mostly based on steady state conditions. Moreover, the model complexity dramatically increases after one packs up the single-cell models into the stack model. These models usually require very high computational cost and cannot be used in online monitoring that needs *real-time* prediction. In order to establish a tractable stack model that can be directly used in health monitoring, here we use the control volume (CV) approach at the modeling stage. The aforementioned benchmark stack is divided into seven groups, each of which is composed of five cells. The fuel cell sub-group is divided into three control volumes, the anode channel, the cathode channel, and the fuel cell body. As each fuel cell sub-group is composed of five single fuel cells, the five anode channels involved in this sub-group are treated as one anode channel CV. Same is applied to the cathode channel CV and the fuel cell body CV. For a sub-group composed of five single fuel cells, the species conservation and energy conservation principles are applied to three CVs [14]. If pure hydrogen is used as fuel and is humidified before entering the anode channel, two species, i.e., hydrogen and water (liquid and vapor), will be involved in the modeling. There are three equations for mass conservation and one equation for energy conservation. It is worth mentioning that phase change plays a critical role in PEM fuel cell operations. This is especially relevant in a model-based condition modeling because the water content and heat directly decide the proper operation of a PEM fuel cell. The present model explicitly takes this into account.

2.2.1. Anode channel

Mass conservation:

$$\frac{\mathrm{d}m_{\mathrm{H_2}}}{\mathrm{d}t} = W_{\mathrm{H_2,in}} - W_{\mathrm{H_2,out}} - M_{\mathrm{H_2}}\frac{NI}{2F} \tag{1}$$

$$\frac{\mathrm{d}m_{\mathrm{an,v}}}{\mathrm{d}t} = W_{\mathrm{an,v,in}} - W_{\mathrm{an,v,out}} - W_{\mathrm{v,mem}} + \{\mathrm{sgn}\}_{\mathrm{p}} W_{\mathrm{an,v,phase}} \tag{2}$$

$$\frac{\mathrm{d}m_{\mathrm{an,w}}}{\mathrm{d}t} = -\{\mathrm{sgn}\}_{\mathrm{p}} W_{\mathrm{an,v,phase}} - W_{\mathrm{an,w,out}} \tag{3}$$

All notations are defined in the Nomenclature. In the above equations, the hydrogen inlet flow rate $W_{\mathrm{H_2,in}}$ depends on the source fuel and anode channel pressure, relative humidity, temperature, and anode inlet flow rate coefficient. The flow rates of other species, $W_{\mathrm{H_2,out}}$, $W_{\mathrm{an,v,in}}$, $W_{\mathrm{an,v,out}}$, and $W_{\mathrm{an,w,out}}$, can be obtained similar to $W_{\mathrm{H_2,in}}$. $W_{\mathrm{v,mem}}$ is the water flow rate across the membrane that can be calculated based on the electro-osmotic drag force and the back-diffusion from the cathode side to the anode side caused by the water content difference [16,17].

In Eqs. (2) and (3), the sign function $\{\mathrm{sgn}\}_{\mathrm{p}}$ is used to characterize the direction of phase change, (+1) indicating evaporation and (−1) indicating condensation. It is worth mentioning that the two-phase change is an important feature in PEM fuel cells that operate at relatively low temperatures. It plays an important role in heat and water management, and humidification of membrane and electro-catalyst layers [14]. In literature, various modeling approaches have been proposed to characterize this phenomenon. In microscopic level modeling, multi-phase mixture based two-phase flow model is employed, where the phases are assumed to be distinct and separable components with non-zero interfacial areas, and the phase change is characterized by smoothly varying phase compositions in their mixture [18,19]. Such micro-level models generally reflect the local behavior only and require very high computational cost which is not feasible for online applications. There has been recent interest

in developing system-level models that can provide the global characterization of the system behavior [14,16]. Pukrushpan et al. [16] developed a constant temperature model where it was assumed that the vapor condenses into the liquid form once the relative humidity of the gas exceeds 100%. Xue and Tang [14] proposed a phase change modeling approach, which is incorporated into a comprehensive system-level dynamic model of PEM fuel cells. The fundamental principle is that if the vapor partial pressure is larger than the in situ saturation vapor pressure, liquid water will be formed through condensation. On the other hand, if the vapor partial pressure is smaller than the corresponding in situ saturation pressure, the existent liquid water will evaporate until the vapor partial pressure reaches the saturation pressure. In this study, we employ this modeling approach, and the phase change rate equation is given as [14]

$$W_{\mathrm{an,v,phase}} = \frac{V_{\mathrm{an}}}{R_{\mathrm{v}} T_{\mathrm{an}}} \frac{1}{\tau(T_{\mathrm{an}}, P_{\mathrm{an,v}}, \alpha_{\mathrm{an}})} (P^{T_{\mathrm{an}}}_{\mathrm{an,v,sat}} - P_{\mathrm{an,v}})$$

where V_{an} is the channel volume of the sub-group.

Energy conservation:

$$\begin{aligned} \frac{\mathrm{d}}{\mathrm{d}t}\left[\left(\sum_i m_i c_i\right) T_{\mathrm{an}}\right] &= \sum_j W_{j,\mathrm{in}} T_{\mathrm{s,an}} - \sum_j W_{j,\mathrm{out}} T_{\mathrm{an}} \\ &- M_{\mathrm{H_2}} \frac{NI}{2F} c_{\mathrm{p,H_2}} T_{\mathrm{an}} + \{\mathrm{sgn}\}_{\mathrm{p}} W_{\mathrm{an,v,phase}}(-h_{\mathrm{latent}}) \\ &+ (hA)_{\mathrm{an}}(T_{\mathrm{body}} - T_{\mathrm{an}}) - W_{\mathrm{v,mem}} c_{\mathrm{p,v}}[\{\mathrm{sgn}\}_{\mathrm{d}} T_{\mathrm{an}} \\ &+ (\{\mathrm{sgn}\}_{\mathrm{d}} - 1) T_{\mathrm{body}}] \end{aligned} \tag{4}$$

where the sign function $\{\mathrm{sgn}\}_{\mathrm{d}}$ is used to indicate the vapor transport direction in MEA, $\{\mathrm{sgn}\}_{\mathrm{d}} = +1$ if vapor is transported from the anode channel to the cathode channel, and $\{\mathrm{sgn}\}_{\mathrm{d}} = 0$ otherwise. $(hA)_{\mathrm{ca}}$ represents the convective heat transfer coefficient between the cathode channel control volume and the fuel cell body.

2.2.2. Cathode channel

Mass conservation:

$$\frac{\mathrm{d}m_{\mathrm{O_2}}}{\mathrm{d}t} = W_{\mathrm{O_2,in}} - W_{\mathrm{O_2,out}} - M_{\mathrm{O_2}} \frac{NI}{4F} \tag{5}$$

$$\begin{aligned} \frac{\mathrm{d}m_{\mathrm{ca,v}}}{\mathrm{d}t} &= W_{\mathrm{ca,v,in}} - W_{\mathrm{ca,v,out}} + M_{\mathrm{v}} \frac{NI}{2F} + W_{\mathrm{v,mem}} \\ &+ \{\mathrm{sgn}\}_{\mathrm{p}} W_{\mathrm{ca,v,phase}} \end{aligned} \tag{6}$$

$$\frac{\mathrm{d}m_{\mathrm{ca,w}}}{\mathrm{d}t} = -\{\mathrm{sgn}\}_{\mathrm{p}} W_{\mathrm{ca,v,phase}} - W_{\mathrm{ca,w,out}} \tag{7}$$

Energy conservation:

$$\begin{aligned} \frac{\mathrm{d}}{\mathrm{d}t}\left[\left(\sum_i m_i c_i\right) T_{\mathrm{ca}}\right] &= \sum_j W_{j,\mathrm{in}} T_{\mathrm{s,ca}} - \sum_j W_{j,\mathrm{out}} T_{\mathrm{ca}} \\ &- M_{\mathrm{O_2}} \frac{NI}{4F} c_{\mathrm{p,O_2}} T_{\mathrm{ca}} + M_{\mathrm{v}} \frac{NI}{2F} c_{\mathrm{p,v}} T_{\mathrm{body}} + (hA)_{\mathrm{ca}}(T_{\mathrm{body}} - T_{\mathrm{ca}}) \\ &+ W_{\mathrm{v,mem}} c_{\mathrm{p,v}}[\{sgn\}_{\mathrm{d}} T_{\mathrm{body}} + (1 - \{\mathrm{sgn}\}_{\mathrm{d}}) T_{\mathrm{ca}}] \\ &+ \{\mathrm{sgn}\}_{\mathrm{p}} W_{\mathrm{ca,v,phase}}(-h_{\mathrm{latent}}) \end{aligned} \tag{8}$$

2.2.3. Fuel cell body

The fuel cell body is treated as a solid control volume. The mass of the fuel cell body is assumed to be a constant, and thus the mass conservation is trivial. The only concerned dynamic behavior of fuel cell body is the temperature. Using the energy conservation, we have

$$\begin{aligned} m_{\mathrm{body}} c_{\mathrm{body}} \frac{\mathrm{d}T_{\mathrm{body}}}{\mathrm{d}t} &= M_{\mathrm{H_2}} \frac{NI}{2F} c_{\mathrm{p,H_2}} T_{\mathrm{an}} + M_{\mathrm{O_2}} \frac{NI}{4F} c_{\mathrm{p,O_2}} T_{\mathrm{ca}} \\ &- M_{\mathrm{H_2O}} \frac{NI}{2F} c_{\mathrm{p,H_2O}} T_{\mathrm{body}} + W_{\mathrm{v,mem}} c_{\mathrm{p,H_2O}}[\{\mathrm{sgn}\}_{\mathrm{an}} T_{\mathrm{an}} \\ &- T_{\mathrm{body}} + (1 - \{\mathrm{sgn}\}_{\mathrm{an}}) T_{\mathrm{ca}}] + NI^2 R_{\mathrm{ohm}} + \Delta H \left(M_{\mathrm{H_2}} \frac{NI}{2F}\right) \\ &- NV_{\mathrm{cell}} I + (hA)_{\mathrm{an}}(T_{\mathrm{an}} - T_{\mathrm{body}}) + (hA)_{\mathrm{ca}}(T_{\mathrm{ca}} - T_{\mathrm{body}}) \\ &+ (hA)_{\infty}(T_{\infty} - T_{\mathrm{body}}) + (hA)_{\mathrm{cw}}(T_{\mathrm{cw}} - T_{\mathrm{body}}) \\ &+ (\mathrm{KA})(T^{i-1}_{\mathrm{body}} - 2T^{i}_{\mathrm{body}} + T^{i+1}_{\mathrm{body}}) \end{aligned} \tag{9}$$

If the water is transported from the anode side to the cathode side, i.e., $\{\mathrm{sgn}\}_{\mathrm{an}} = 1$, the anode channel temperature has contribution to the fuel cell temperature change. Otherwise, $\{\mathrm{sgn}\}_{\mathrm{an}} = 0$, and it is the cathode channel temperature T_{ca} that will affect the fuel cell temperature. The last term in Eq. (9) represents the conduction heat transfer among the neighboring sub-groups.

2.2.4. Electrochemical reaction

Typically, the fuel cell output voltage is the summation of three effects [16], the Nernst potential, the cathode and anode activation overvoltage, and the ohmic overvoltage due to internal resistance,

$$V_{\mathrm{cell}} = E_{\mathrm{Nernst}} - \eta_{\mathrm{act}} - \eta_{\mathrm{ohmic}} \tag{10}$$

where the Nernst potential, the activation voltage and the ohmic voltage loss are functions of the operating conditions. One way of modeling the activation overvoltage and ohmic overvoltage is to take into account that the membrane conductivity is strongly dependent upon the membrane water content and fuel cell temperature [20]. Alternatively, the expressions of the activation overvoltage and the ohmic overvoltage may be characterized using the experimental data under various cell temperature and load current [13,14,16],

$$\eta_{\mathrm{act}} = -\xi_1 - \xi_2 T_{\mathrm{body}} - \xi_3 T_{\mathrm{body}} \ln(c^*_{\mathrm{O_2}}) - \xi_4 T_{\mathrm{body}}(I) \tag{11}$$

$$\eta_{\mathrm{ohmic}} = I(\xi_5 + \xi_6 T_{\mathrm{body}} + \xi_7 I) \tag{12}$$

where $c^*_{\mathrm{O_2}}$ is the concentration of oxygen at the catalyst interface, and ξ_i ($i = 1, \ldots, 7$) are parameters calculated from the experimental data using linear regression. It should be noted that the electrochemical effects may vary slightly from cell to cell and depend on the complicated operating conditions within a cell. In order to take into account the system variation/uncertainty, in this research we use the linear regression expressions where the coefficients can be easily perturbed during the statistical sampling.

As the cells are serially connected, the sub-group output voltage will be the summation of the five single cell output voltages.

2.2.5. Stack model assembly

Eqs. (1)–(12) provide a basis for the modeling of the concerned fuel cell sub-group. The assembly of such sub-group systems will form the stack model, which also include heat conduction effect among these fuel cell sub-groups. As the total inlet flow rate of fuel/gas is individually fed into each of the fuel cells and the exhaustion of each fuel cell converges to the stack outlet, the inlet/outlet flow rates of the stack will be the summation of the respective sub-group inlet/outlet flow rates. The cooling water flow rate is treated in the same manner. We then have,

$$W_{\text{total},\text{H}_2,\text{in}} = \sum_{i=1}^{7} W_{i,\text{H}_2,\text{in}}, \tag{13a}$$

$$W_{\text{total},\text{H}_2,\text{out}} = \sum_{i=1}^{7} W_{i,\text{H}_2,\text{out}} \tag{13b}$$

$$W_{\text{total},\text{O}_2,\text{in}} = \sum_{i=1}^{7} W_{i,\text{O}_2,\text{in}}, \tag{14a}$$

$$W_{\text{total},\text{O}_2,\text{out}} = \sum_{i=1}^{7} W_{i,\text{O}_2,\text{out}} \tag{14b}$$

$$W_{\text{total,cw}} = \sum_{i=1}^{7} W_{i,\text{cw}} \tag{15}$$

In all, there are seventy first-order dynamic equations for the stack. A variety of stack state variables can be obtained from the model simulation. In this study, the sub-group output voltage will be employed to monitor the conditions of the stack using the Hotelling statistical analysis.

2.3. Baseline simulation with system uncertainties

In the aforementioned dynamic model, all the system parameters are assumed as deterministic parameters. However, in a real fuel cell system, variations/uncertainties exist. Part of the uncertainties comes from the normal time-evolution nature of fuel cell components as well as the cell-to-cell manufacturing variation. From the modeling perspective, even more significant uncertainties may appear since the fuel cell model involves coefficients obtained based on experimental studies (e.g., in Section 2.2.4). PEM fuel cells are highly non-linear. The practical operation of a PEM fuel cell is essentially dynamic and thus the operating conditions cover various combinations of parameters/states that may deviate from the nominal condition. In addition, all the sensor measurements (of the input state variables and the output voltage) may be subjected to noise.

In order to take into account the fuel cell variations/uncertainties effect in the condition monitoring system, in this research we let the key empirical parameters used in the baseline model be random variables with specified statistics (Table 2). As a result, the model outputs become stochastic in nature. Stochastic analysis is a procedure where the input parametric uncertainties propagate through a physical process (such as the fuel cell system). As most of the physical processes in the PEM fuel cell system are governed by differential/partial differential equations and are non-linear processes, the uncertainty propagation using the closed-form result is not feasible. In the proposed condition monitoring system, we will use the sampling approach to perturb the uncertain parameters, which essentially leads to a group of output voltages as the baseline. This group of output voltages covers the possible output range under the normal operation condition, which will be used in the Hotelling T^2 statistics analysis for damage detection.

In traditional stochastic analysis, the samples are selected randomly using such as the Monte Carlo technique [21]. The computational cost for such sampling, however, is in general quite high [21–23]. To improve the sampling efficiency, the stratified sampling methods have been developed, such as the Latin hypercube sampling (LHS) method [24] and the Hammersley sequence sampling (HSS) method [25]. The LHS method is a stratified sampling method, where the distribution is divided into m intervals with equal probability, and the sample is then picked randomly from each interval. In the HSS method, m sampling points are uniformly placed in a k-dimensional cube through a low-discrepancy design, and the representative sample is generated. In order to demonstrate the proposed condition monitoring strategy, here we assume that the empirical parameters listed in Table 2 all have the Gaussian distribution, and the corresponding standard deviations are also listed in the same table. Let the total number of uncertain parameters be q. Using the LHS procedure, m values of each of the parameters are sampled under the Gaussian distribution assumption. We then obtain a $m \times q$ sampling data matrix. For each column data, the m values are randomly distributed with one from each interval as mentioned above, and they are randomly permuted. When a set of the input measurement data (from physical fuel cell system) comes in, the system model will be simulated m times using each row of the above $m \times q$ sampling data matrix. Correspondingly, we will obtain m output voltages, which will be used as the baseline for damage detection. Clearly, these m output data will cover the uncertainty band resulted from the system parameter uncertainty propagation through the system model, and the computational time is reduced using the LHS procedure for sampling.

2.4. Hotelling T^2 statistical analysis for stack condition monitoring

The multiple simulations of PEM stack model under statistical sampling of parametric uncertainties will yield multiple output voltage time-responses as the baseline. These voltage responses (as functions of time, due to the dynamic nature of the PEM fuel cell) will then be compared with the real-time measurement of the output voltage for condition monitoring. Hotelling first proposed the multi-variate statistical analysis for conformity check [10]. This method is considered robust and highly sensitive for such task, and has been widely used in process control and fault detection [11,12]. The analysis is based

upon the T^2 statistics and the comparison with certain control limits.

In general, for a p-variable problem with each variable having m observations, the mean vector is defined as,

$$\bar{\boldsymbol{x}} = [\bar{x}_1, \bar{x}_2, \ldots, \bar{x}_p]^{\mathrm{T}} \tag{16}$$

where $\bar{x}_j = (1/m)\sum_{i=1}^{m} x_{ij}$ is the mean estimation for the j-th variable. The sample covariance matrix S can be calculated as,

$$S = \frac{1}{m-1}\sum_{i=1}^{m}(\boldsymbol{x}_i - \bar{\boldsymbol{x}})(\boldsymbol{x}_i - \bar{\boldsymbol{x}})^{\mathrm{T}} \tag{17}$$

The covariance matrix S indicates the relationship existing among the p-variables. In the present study, the output voltage of each sub-group is used as the information carrier for condition monitoring. Therefore, the output voltage history calculated or measured/sampled will be grouped, with each group having p time points. We will perform condition monitoring based on these grouped p-variables successively. Recall that in order to take into account the system uncertainties caused by the empirical modeling, the fuel cell model will be simulated multiple times with statistical sampling (through the LHS procedure) of physical parameters. We may then obtain m voltage output observations correspondingly. There are two distinct phases involved in constructing the Hotelling T^2 control limits [10]. First, we use the aforementioned m observations (simulations) of healthy fuel cell model to establish a Phase I baseline and an upper control limit under a specified confidence level. The purpose is to examine the baseline data and also the relation of normal condition with respect to the upper control limit. For a given voltage output simulation/observation $\mathbf{x}_i$, the statistic T^2 is defined as

$$T^2 = (\boldsymbol{x}_i - \bar{\boldsymbol{x}})^{\mathrm{T}} S^{-1} (\boldsymbol{x}_i - \bar{\boldsymbol{x}}) \tag{18}$$

It can be proved that the statistic T^2 follows the F-distribution. Therefore, under a given Type 1 error probability α, the Phase I upper control limit $\mathrm{UCL}^1_{p,m,\alpha}$ can be established as [10]

$$\mathrm{UCL}^1_{p,m,\alpha} = \frac{p(m-1)^2}{m(m-p)} F_\alpha(p, m-p) \tag{19}$$

where $F_\alpha(p, m-p)$ is the $1-\alpha$ percentile of the F-distribution with p and $m-p$ degrees of freedom. Indeed, we may use m observations of the output voltage under normal operating condition predicted by the fuel cell model to establish a control limit with $1-\alpha$ confidence level. At this Phase I stage, the observations of normal fuel cell output (obtained by model prediction under statistical sampling) will undergo a self-checking procedure. The statistic T^2 of every output voltage prediction will be compared with the upper control limit. If the statistic T^2 of certain prediction exceeds the upper control limit, we may either eliminate this prediction from the baseline data or revise the upper control limit (and, correspondingly, the confidence level). This procedure iterates until the baseline data are purified.

The baseline output voltages under normal operating condition will then be utilized to establish Phase II statistic T^2 for condition monitoring. This is facilitated by incorporating the real-time online measurement of fuel cell output voltage into the analysis. Since the new voltage measurement is independent of the Phase I baseline, the Phase II upper control limit is modified as [10]

$$\mathrm{UCL}^2_{p,m,\alpha} = \frac{p(m-1)(m+1)}{m(m-p)} F_\alpha(p, m-p) \tag{20}$$

In other words, when a real-time measurement of output voltage comes in, we need to use Eq. (18) to calculate the statistic T^2 value of this new p-variable. If this value exceeds the Phase II upper control limit that we have established in Eq. (20), we may conclude, with $1-\alpha$ confidence level, that the voltage output is abnormal and fault condition has occurred in the corresponding sub-group of the stack. From the above procedure, we can see that the Hotelling T^2 analysis allows the direct comparison of

Table 1
Parameters used in the model validation and simulation

Parameters	Value	Reference
$K_{\mathrm{an,in}}$ (kg(Pa s)$^{-1}$)	1.23×10^{-10}	[a]
$P_{\mathrm{s}}^{\mathrm{an}}$ (psig)	35	[13]
$T_{\mathrm{an,in}}$ (°C)	23.5	[13]
φ_{an}	0.9	[b]
$K_{\mathrm{ca,out}}$ (kg(Pa s)$^{-1}$)	2×10^{-5}	[a]
$T_{\mathrm{ca,in}}$ (°C)	23.5	[13]
φ_{ca}	0.0	[b]
W_{cw} (kg s^{-1})	0.0331568	[13]
m_{cw} (kg)	2.5	[b]
$(hA)_{\mathrm{an}}$ (W K^{-1})	2	[13]
$(hA)_{\infty}$ (W K^{-1})	17	[13]
T_{∞} (°C)	23.5	[13]
t_m (m)	1.275×10^{-4}	[16]
$\rho_{m,\mathrm{dry}}$ (kg cm^{-3})	0.002	[1]
$K_{\mathrm{an,out}}$ (kg(Pa s)$^{-1}$)	2×10^{-5}	[a]
P_{atm} (Pa)	1.013×10^{5}	[13]
V_{an} (m^3)	0.005	[16]
$K_{\mathrm{ca,in}}$ (kg(Pa s)$^{-1}$)	9.148×10^{-10}	[a]
$P_{\mathrm{s}}^{\mathrm{ca}}$ (psig)	35	[13]
V_{ca} (m^3)	0.01	[16]
MC (J K^{-1})	35000	[13]
$T_{\mathrm{cw,in}}$ (°C)	23.5	[13]
N	35	[13]
$(hA)_{\mathrm{ca}}$ (W K^{-1})	10	[13]
$(hA)_{\mathrm{cw}}$ (W K^{-1})	50	[13]
τ (s)	30	[b]
A_{cell} (m^2)	0.0232	[13]
$M_{m,\mathrm{dry}}$ (kg mol^{-1})	1.1	[1]

[a] Coefficients are so chosen that the fuel/gas inlet flow rate is the same as those of the experimental setup.
[b] Parameters are assumed.

Table 2
Parameters used in the simulation and uncertainties

Parameters	Value	Standard deviation (%)	Reference
ξ_1	0.944	0.01	[13] for mean value
ξ_2	-3.54×10^{-3}	0.1	[13] for mean value
ξ_3	-4.68×10^{-4}	0.1	[13] for mean value
ξ_4	1.96×10^{-4}	0.1	[13] for mean value
ξ_5	-3.3×10^{-3}	0.1	[13] for mean value
ξ_6	7.55×10^{-6}	0.1	[13] for mean value
ξ_7	-1.1×10^{-6}	0.1	[13] for mean value

the online measurement with a group of possible output voltage under normal operation conditions, which is a key feature of the proposed condition monitoring strategy.

3. Simulation and discussion

3.1. Dynamic simulation of fuel cell stack using nominal parameters

In order to explore the dynamic behavior of the PEM fuel cell stack under various fault conditions, a series of step changes in load current is applied to the fuel cell system to emulate the external load change. The initial conditions and system parameters are listed in Tables 1 and 2. Here in this first study, we assume an ideal system without uncertainties, and hence all system parameters take the nominal values. The purpose is to compare the nominal difference of fuel cell state variables caused by the fault conditions. During the simulation, the fault condition is deliberately introduced into the system. The total time period for the simulation is 30,000 s. Initially, no external load current is applied to the system. At the 100th s, the system starts up with a 20 A external load current. At the 5000th s, the membrane drying of a single cell is introduced into sub-groups 3 and 6, respectively. This fault condition recovers to the normal condition at the 7000th s. At the 11,000th s, the load current continuously rises up to 30 A. The cathode flooding is then introduced to a single cell in sub-group 6 at the 17,000th s which continues for 3000 s. The fuel cell then returns to the normal condition. The last fault introduced is the cathode flooding of a single cell of sub-group 3 at the 25,000th s. A number of stack state variable histories are shown in Figs. 2–13.

We first analyze the fuel cell state variable histories to gain the physical insight. Fig. 2 shows the stack temperature history. All seven sub-groups show similar trend, i.e., the stack temperature increases following the increase of the external load current. The temperature is influenced by the occurrence of cell faults. At the 5000th s, the membrane drying is introduced into sub-groups 3 and 6, respectively, and the drying level of sub-group 3 is higher

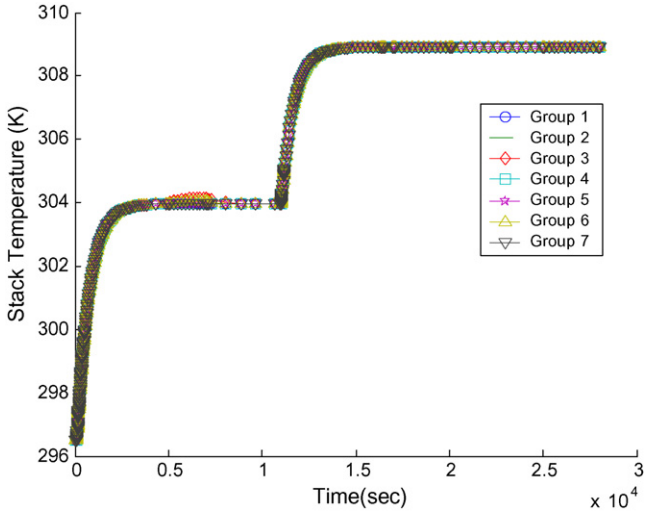

Fig. 2. Stack temperature history simulation.

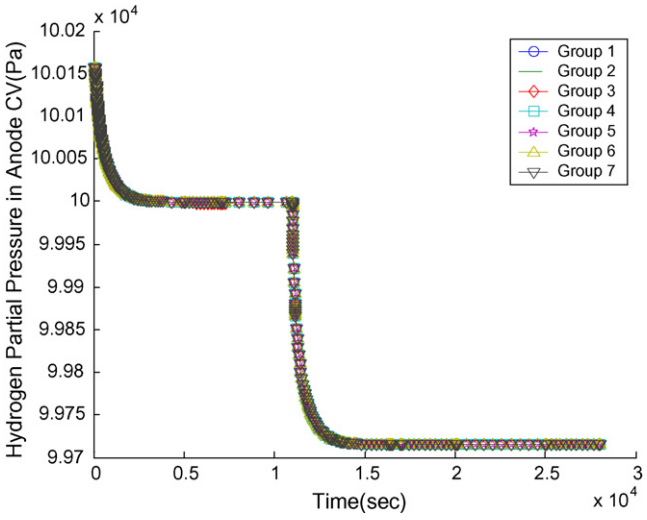

Fig. 3. Fuel partial pressure simulation in anode CV.

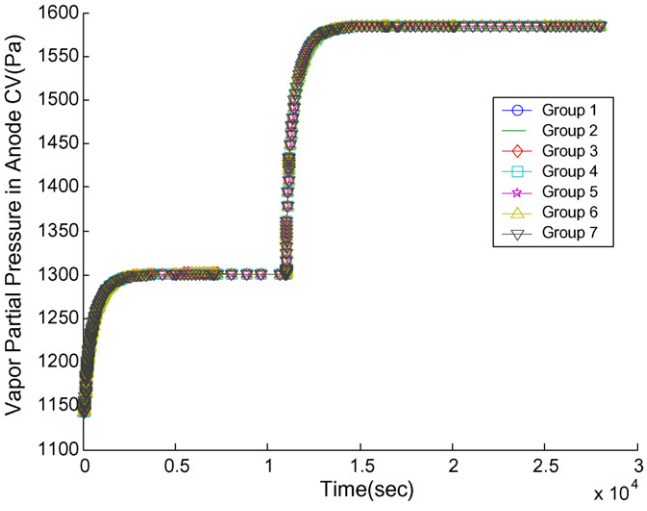

Fig. 4. Vapor partial pressure simulation in anode CV.

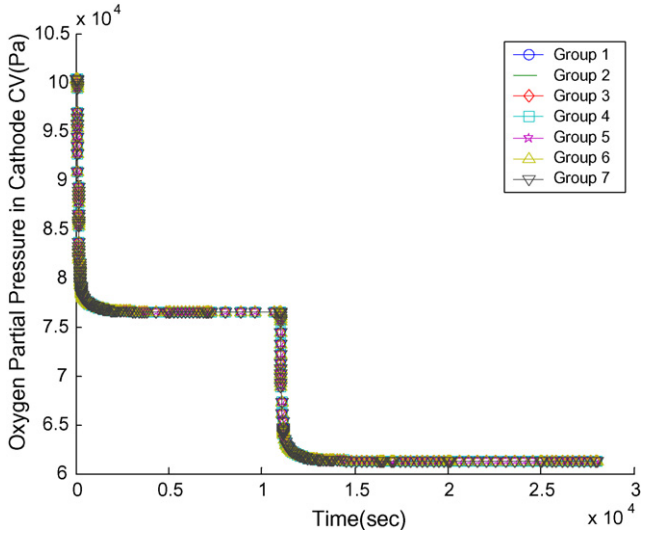

Fig. 5. Oxygen partial pressure simulation in cathode CV.

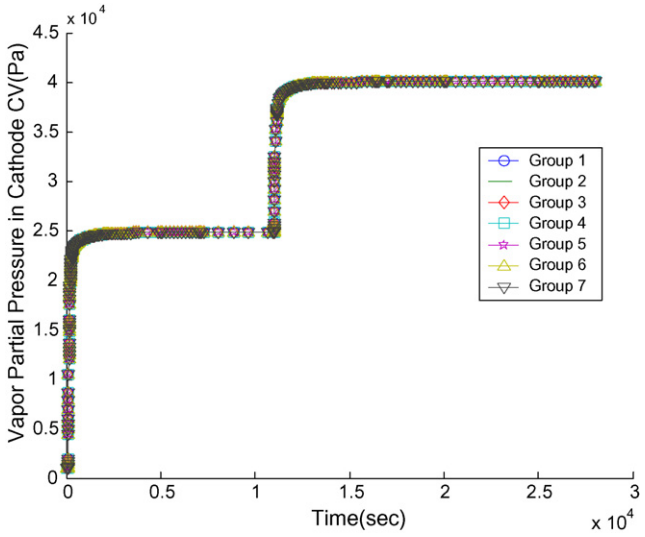

Fig. 6. Vapor partial pressure simulation in cathode CV.

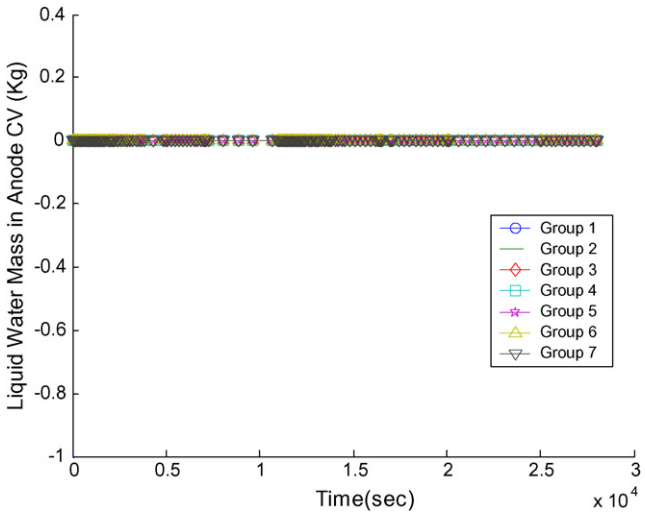

Fig. 7. Liquid water mass simulation in anode CV.

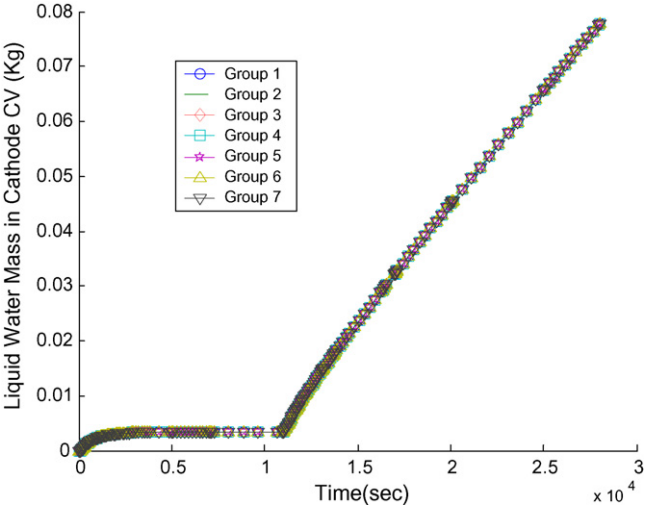

Fig. 8. Liquid water mass simulation in cathode CV.

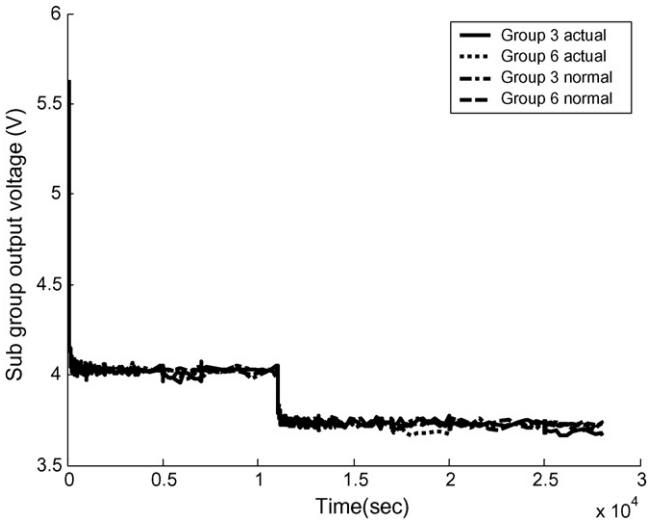

Fig. 9. Direct comparison of sub-group voltage values.

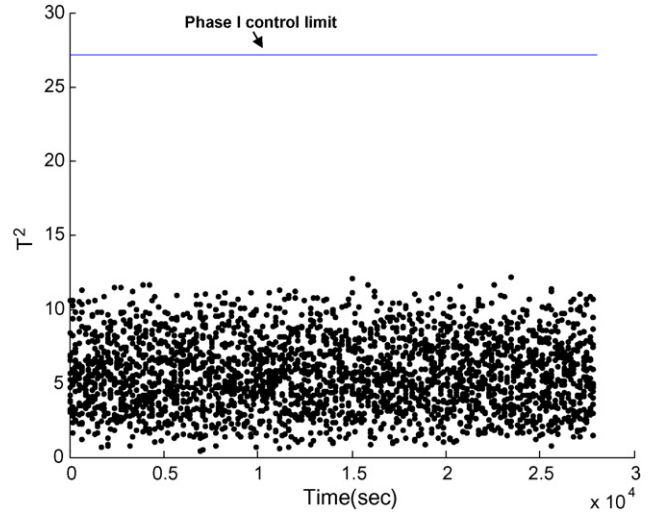

Fig. 10. Baseline self-checking result of sub-group 3 voltage.

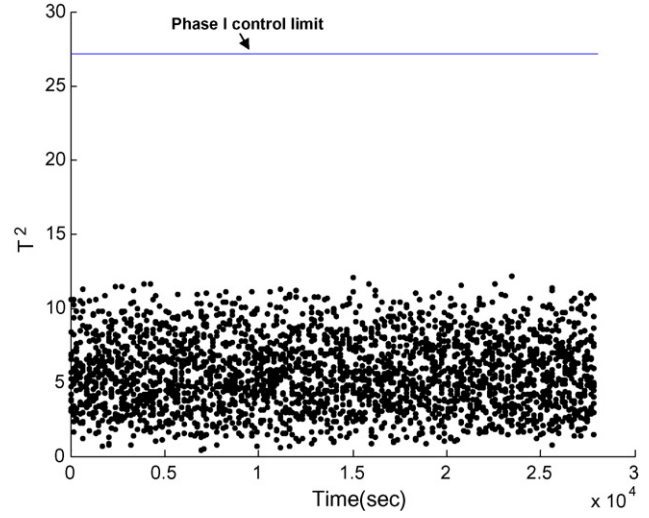

Fig. 11. Baseline self-checking result of sub-group 6 voltage.

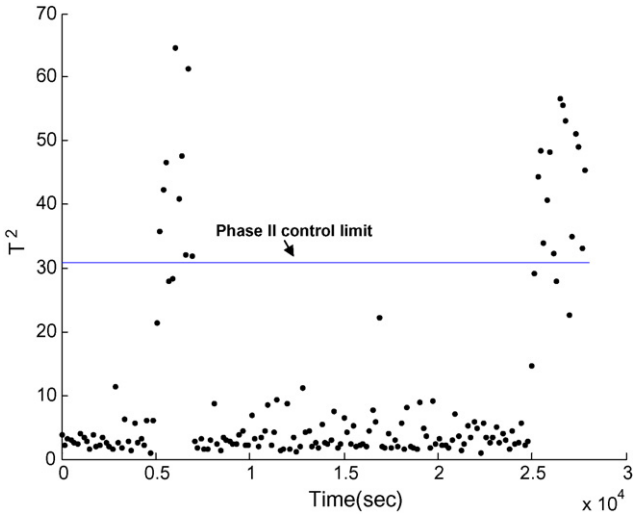

Fig. 12. Hotelling analysis of sub-group 3 voltage.

than that of the sub-group 6. It is apparent that temperatures of sub-groups 3 and 6 both increase with sub-group 3 having a higher temperature. Similarly, the flooding of cathode electrode blocks the transport of oxygen from the cathode channel to the cathode electrolyte and, consequently, the oxygen partial pressure at the electrolyte decreases, which directly leads to the output voltage decrease. Here it is assumed that the oxygen at the electrolyte is adequate for the electrochemical reaction under the loading conditions. The decrease of the electrical power leads to the temperature increase of sub-groups 3 and 6, provided that the consumed fuel is the same as that of the normal operating conditions. This result is shown in Fig. 2 at the 17,000th and 25,000th s, respectively. One may observe that the temperature increase of sub-groups 3 and 6 influences the neighboring stack temperature.

Figs. 3 and 4 show the hydrogen and vapor partial pressures in the anode channel CV of seven sub-groups. The hydrogen partial pressure tends to go down following the load current increase. The increase of the load current directly leads to the increase

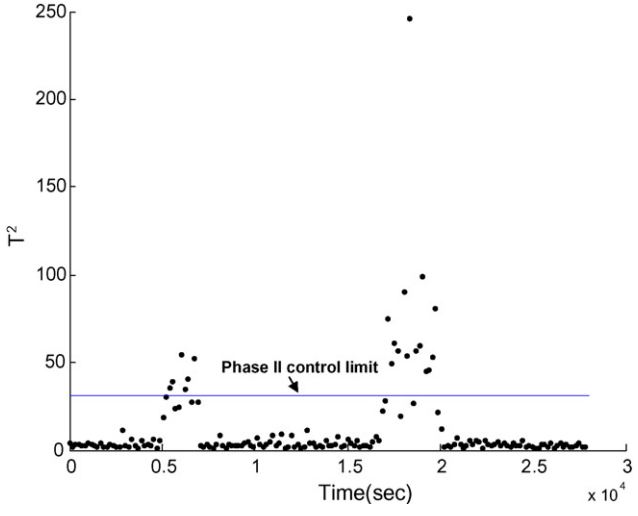

Fig. 13. Hotelling analysis of sub-group 6 voltage.

of the consumed fuel and water generated due to the electrochemical reaction. Consequently, the hydrogen partial pressure in the anode CV decreases even though the anode CV temperature increases, while the partial pressure of the vapor increases due to both anode CV temperature increase and the increase of water diffusion effect from the cathode side to the anode side. In Figs. 5 and 6, the oxygen and vapor partial pressures in the cathode show similar trends to those of the anode CV.

Figs. 7 and 8 illustrate the liquid water generated due to phase change in the anode and cathode CVs, respectively. It is apparent that there is no liquid water in the anode CV, while the liquid water generated in the cathode CV increases following the increase of the external load current. Clearly, as the electrochemical reaction intensifies, the water vapor generated increases and then the condensation takes place in the cathode CV. One may see that the faults are explicitly simulated using the above developed model, and they do cause some interesting changes during fuel cell operations.

3.2. Hotelling monitoring

In this sub-section, we demonstrate the Hotelling statistical analysis method for fault detection. As stated, under the respective fault conditions in three time periods (5000th–7000th s, cells in sub-groups 3 and 6 having faults; 17,000th–20,000th s, a cell in sub-group 6 having fault; 25,000th–28,000th s, a cell in sub-group 3 having fault), the output voltages of sub-groups have very small fault-caused variations relative to the healthy condition (the exact maximum variation using nominal parameters without uncertainty is 0.0446 V). In practical applications, the healthy responses are subjected to model uncertainty, and both the healthy and faulty responses will be contaminated by measurement noise. In this research, the modeling uncertainty is accounted for by assuming variance in the empirical parameters used in the description of electrochemical reaction (Table 2). It should be noted that little knowledge currently exists in quantifying such uncertainty, and the standard deviation values shown in Table 2 are obtained by trial and error that yield reasonable output voltage history calculation in the simulation. In future, comprehensive experiments are needed in quantifying such uncertainty. In addition to such parametric uncertainties, in this study we assume that the voltage measurement is subjected to random noise with 0.016 V standard deviation. Fig. 9 illustrates the output voltages of the faulty sub-groups 3 and 6, respectively. Also shown are the healthy output voltages selected from the corresponding baseline (obtained via statistical sampling, which will be further discussed later) under the same operating conditions. Clearly, the fault conditions cause very insignificant change of output voltage, which is further contaminated by the noise. Therefore, it is virtually impossible to declare fault occurrence based upon the direct comparison of output voltages, as shown in Fig. 9.

We then implement the Hotelling statistic T^2 detection method, where we use sampled output voltage measurements as the p-variable. Here, for easy identification of the fault sources, the Hotelling detection is applied for each sub-group of the voltages. In order to establish the baseline and the control limit,

a set of fuel cell output voltages are generated using the fuel cell model under statistical sampling of parametric uncertainties (through the LHS procedure) under the normal operating conditions. Here, the Gaussian distributions are assumed for the uncertain parameters (shown in Table 2) and each distribution is divided into 16 strata. Output voltages are grouped every 6 time points, i.e., $p = 6$. Hotelling analysis are performed successively for the entire voltage histories. After self-checking, a baseline composed of 16 sample voltages is constructed. Figs. 10 and 11 show the corresponding self-checking results of normal voltage outputs of sub-groups 3 and 6, respectively. Here, the confidential level of the F-distribution is set to be 95%. The degree of freedom of the Phase I self-checking is $p \times m = 6 \times 16$. The upper control limit of Phase I is 27.14. Clearly, the self-checking results of the baseline are below the Phase I upper control limit, and we may now declare with 95% confidence that the baseline is purified.

At Phase II, the (simulated) online measurement of sub-group output voltage measurements is inserted into the Hotelling analysis module, and analyzed based on the baseline developed at Phase-I stage. If the statistic T^2 of the online output voltage measurement exceeds the Phase II upper control limit, a fault condition can be declared; otherwise, the operating condition is treated as normal. Again, each subgroup output voltage of the online fuel cell output voltage is consecutively grouped for every 6 time points. One advantage of this strategy is that the condition monitoring system would have enough time to process all the calculations. With the new online measurement, the Phase II upper control limit can be calculated as 30.76 under a 95% confidence level (Eq. (20)). We then test this condition monitoring method by incorporating the simulated voltage measurement of the faulty fuel cell system. Figs. 12 and 13 show the Hotelling results of abnormal voltage outputs of sub-groups 3 and 6, respectively. It can be clearly seen that the T^2 values of the measurements exceed the upper control limit at the time instant when the fault occurs. The Hotelling statistic T^2 of sub-groups 3 and 6 declare both fault at the 5000th s. The fault condition lasts for about 2000 s and then the T^2 values drop to below the upper control limit. At the 17,000th s, the Hotelling statistic T^2 of sub-group 6 goes beyond the upper control limit, which lasts for 3000 s. At the 25,000th s, the Hotelling statistic T^2 of sub-group 3 declares fault condition. While the direct comparison of the fault and normal voltages in Fig. 9 cannot give definitive conclusion, the Hotelling method significantly improves the detection sensitivity and can correctly predict the fault occurrence immediately, even under system parameter uncertainties and noisy measurements.

4. Concluding remarks

This research proposes a condition monitoring approach for the PEM fuel cells. The basic idea is to compare the fuel cell output voltage measurement with model prediction under the same operating conditions. We first develop a fuel cell stack model which can simulate the complicated transient behavior and dynamic interaction of the temperature, gas flow, phase change in the anode and cathode channels, and membrane humidification under operating conditions. Using this model as basis, we then simulate the stack output voltage response, where statistical sampling is incorporated to account for the system uncertainties. This yields a group of output voltage histories as the baseline. We finally employ the Hotelling T^2 control limit approach to monitor the stack condition by statistically comparing the voltage measurement with the baseline voltages. Our analysis indicates that this Hotelling method has very high detection sensitivity and can detect the fault conditions at the early stage.

Acknowledgements

This research is supported by the NASA Connecticut Space Grant Consortium under a Workforce Development Grant, by NSF under grants CMS-0428210 and CMS-0427878, and by NEDO as part of the Advanced Ceramic Reactor Project. The authors thank the anonymous reviewers for their helpful suggestions.

References

[1] T.V. Nguyen, R.E. White, A water and heat management model for proton-exchange-membrane fuel cells, J. Electrochem. Soc. 140 (1993) 2178–2186.
[2] T.E. Springer, T.A. Zawodzinski, S. Gottesfeld, polymer electrolyte fuel cell model, J. Electrochem. Soc. 138 (1991) 2334–2342.
[3] T.E. Springer, M.S. Wilson, S. Gottesfeld, Modeling and experimental diagnostics in polymer electrolyte fuel cells, J. Electrochem. Soc. 140 (1993) 3513–3526.
[4] P. Rodatz, F. Buchi, C. Onder, L. Guzzella, Operational aspects of a large PEFC stack under practical conditions, J. Power Sources 128 (2004) 208–217.
[5] H.H. Voss, D.P. Wilkinson, P.G. Pickup, M.C. Johnson, V. Basura, Anode water removal: a water management and diagnostic technique for solid polymer fuel cells, Electrochim. Acta 40 (1995) 321–328.
[6] D.L. Wood III, J.S. Yi, T.V. Nguyen, Effect of direct liquid water injection and interdigitated flow field on the performance of proton exchange membrane fuel cells, Electrochim. Acta 43 (1998) 3795–3809.
[7] T.V. Nguyen, M.W. Knobbe, A liquid water management strategy for PEM fuel cell stacks, J. Power Sources 114 (2003) 70–79.
[8] J.O. Schumacher, P. Gemmar, M. Denne, M. Zedda, M. Stueber, Control of miniature proton exchange membrane fuel cells based on fuzzy logic, J. Power Sources 129 (2004) 143–151.
[9] D. Hissel, M.C. Pera, J.M. Kauffmann, Diagnosis of automotive fuel cell power generators, J. Power Sources 128 (2004) 239–246.
[10] G.A.F. Seber, Multivariate Observations, John Wiley & Sons, New York, NY, 1984.
[11] R.L. Mason, N.D. Tracy, J.C. Young, Decomposition of T^2 for multivariate control chart interpretation, J. Qual. Technol. 27 (1995) 99–108.
[12] J. Jin, J. Shi, Automatic feature extraction of waveform signals for in-process diagnostic performance improvement, J. Intell. Manuf. 12 (2001) 257–268.
[13] J.C. Amphlett, R.F. Mann, B.A. Peppley, P.R. Roberge, A. Rodrigues, A model predicting transient response of proton exchange membrane fuel cells, J. Power Sources 61 (1996) 183–188.
[14] X. Xue, J. Tang, PEM fuel cell dynamic model with phase change effect, ASME J. Fuel Cell Sci. Technol. 2 (2005) 213–294.
[15] S. Um, C.Y. Wang, Three-dimensional analysis of transport and electrochemical reactions in polymer electrolyte fuel cells, J. Power Sources 125 (2004) 40–51.
[16] J.T. Pukrushpan, H. Peng, A.G. Stefanopoulou, Control-oriented modeling and analysis for automotive fuel cell systems, ASME J. Dyn. Syst. Meas. Control 126 (2004) 14–25.

[17] H. Liu, T. Zhou, P. Cheng, Transport phenomena analysis in proton exchange membrane fuel cells, ASME J. Heat Transfer 127 (2005) 1363–1379.
[18] Z.H. Wang, C.Y. Wang, K.S. Chen, Two-phase flow and transport in the air cathode of proton exchange membrane fuel cells, J. Power Sources 90 (2001) 40–50.
[19] L. You, H. Liu, A two-phase flow and transport model for the cathode of PEM fuel cells, Int. J. Heat Mass Transfer 45 (2002) 2277–2287.
[20] S. Dutta, S. Shimpalee, J.W. Van Zee, Numerical predication of mass-exchange between cathode and anode channels in a PEM fuel cell, Int. J. Heat Mass Transfer 44 (2001) 2029–2042.
[21] A. Saltelli, K. Chan, E.M. Scott, Sensitivity Analysis, Wiley, New York, 2000.
[22] D. Bressanini, G. Morosi, Robust wave function optimization procedures in quantum Monte Carlo methods, J. Chem. Phys. 116 (2002) 5345–5350.
[23] M.D. McKay, R.J. Beckman, W.J. Conover, A comparison of three methods for selecting values of input variables in the analysis of output from a computer code, Technometrics 21 (1979) 239–245.
[24] E.J. Pebesma, G.B.M. Heuvelink, Latin hypercube sampling of Gaussian random fields, Technometrics 41 (1999) 303–312.
[25] J. Kalagnanam, U. Diwekar, An efficient sampling technique for off-line quality control, Technometrics 39 (1997) 308–319.